Local delivery of lipid-based nanoparticles containing microbial nucleic acid for osteoimmunomodulation

Rahmani, N. R.; Jahanmard, F.; Hassani Najafabadi, A.; Dogan, O.; Khodaei, A.; Croes, M.; Kruyt, M. C.; Weinans, H.; Amin Yavari, S.; More Authors

DOI
10.1016/j.ejps.2025.107050

Publication date
2025

Document Version
Final published version

Published in
European Journal of Pharmaceutical Sciences

European Journal of Pharmaceutical Sciences 208 (2025) 107050

Contents lists available at ScienceDirect

European Journal of Pharmaceutical Sciences

journal homepage: www.elsevier.com/locate/ejps

Local delivery of lipid-based nanoparticles containing microbial nucleic acid for osteoimmunomodulation

N.R. Rahmani [a,b,1,*], F. Jahanmard [c,1], A. Hassani Najafabadi [d], J. Flapper [c], O. Dogan [c], A. Khodaei [a,b], G. Storm [c], M. Croes [a], M.C. Kruyt [a,e], D. Gawlitta [b,f], H. Weinans [a,g], E. Mastrobattista [c], S. Amin Yavari [a,b,d]

[a] Department of Orthopedics, University Medical Center Utrecht, Heidelberglaan 100, GA 3508, Utrecht, the Netherlands
[b] Regenerative Medicine Center Utrecht, University Utrecht, Heidelberglaan 8, CS 3584, Utrecht, the Netherlands
[c] Department of Pharmaceutics, Utrecht Institute for Pharmaceutical Sciences, Utrecht University, Universiteitsweg 99, CG 3584, Utrecht, the Netherlands
[d] Terasaki Institute for Biomedical Innovation, 21100 Erwin St., Woodland Hills, 91367, Los Angeles, United States
[e] Department of Developmental Biomedical Engineering, Twente University, Drienerlolaan 5, NB 7522, Enschede, the Netherlands
[f] Department of Oral and Maxillofacial Surgery, Prosthodontics and Special Dental Care, University Medical Center Utrecht, Heidelberglaan 100, GA 3508, Utrecht, the Netherlands
[g] Department of Biomechanical Engineering, Technical University Delft, Mekelweg 2, CD 2628, Delft, the Netherlands

ARTICLE INFO

Keywords:
PAMPs
Toll-like receptor
Pathogen recognition receptor
Osteoimmunomodulation
Bone regenerative medicine
In vivo

ABSTRACT

Osteoimmunomodulation is a strategy to promote bone regeneration in implants by modifying the immune environment. CpG-containing oligonucleotides type C (CpG ODN C) and Polyinosinic:polycytidylic acid (Poly[I:C]) are analogs of microbial nucleic acids that have been studied for various immunotherapeutic applications. This research investigates the potential of CpG ODN C and Poly(I:C) as an osteoimmunomodulatory agent for bone regenerative purposes. We encapsulated each nucleic acid in a lipid-based nanoparticle to facilitate the delivery into intracellular pathogen recognition receptors in immune cells. The lipid-based nanoparticles were ±250 nm in size with a negative charge (−36 to −40 mV) and an encapsulation efficiency of ±60 %. Lipid-based nanoparticles containing nucleic acids, Lip/CpG ODN C and Lip/Poly(I:C), increased the production of TNF, IL-6, and IL-10 by primary human macrophages compared to free-form nucleic acids. Conditioned medium from macrophages treated with CpG ODN C (10 μg/ml) and Lip/CpG ODN C (0.1, 1, and 10 μg/ml) promoted osteoblast differentiation of human mesenchymal stromal cells by 2.6-fold and 3-fold, respectively; no effect was seen for Lip/Poly(I:C). Bone implants were prepared, consisting of a biphasic calcium phosphate scaffold, bone morphogenetic protein (BMP) 2, and lipid-based nanoparticles suspended in gelatin methacryloyl (GelMA) hydrogel. Implants were evaluated for *de novo* bone formation in an extra-skeletal implantation model in rabbits for 5 weeks. Based on the particles suspended in GelMA, six groups of implants were prepared: Lip/CpG ODN C, Lip/Poly(I:C), Lip (empty), CpG ODN C, Poly(I:C), and a control group consisting of empty GelMA. After 5 weeks, healthy bone tissue formed in all of the implants with active osteoblast and osteoclast activity, however, the amount of new bone volume and scaffold degradation were similar for all implants. We suggest that the working concentrations of the nucleic acids employed were inadequate to induce a relevant inflammatory response.

Abbreviations: Poly[I:C], Polyinosinic:polycytidylic acid; CpG ODN C, CpG containing oligonucleotides type C; BCP, biphasic calcium phosphate; GelMA, gelatin methacryloyl; BMP-2, bone morphogenetic protein 2; PRR, pattern recognition receptors; PAMP, pathogen-associated molecular pattern; TLR, toll-like receptor; hMSC, human mesenchymal stromal cell; TNF, tumor necrosis factor; IL, interleukin; OSM, oncostatin M; SDF1-α, stromal cell-derived factor 1 alpha; IFN, interferon; CH, cholesterol; DLS, dynamic light scattering; DODAP, 1,2-dioleoyl-3-dimethylammonium-propane; DPPC, 1,2-dipalmitoyl-sn-glycero-3-phosphocholine; DPPG, 1,2-dipalmitoyl-sn-glycero-3-phospho-(1′-rac-glycerol); PDI, Polydispersity index; UV, ultraviolet; Rh-PE, rhodamine B sulfonyl; LPS, lipopolysaccharide; Lip, empty lipid-based nanoparticles; Lip/CpG ODN C, lipid-based nanoparticles containing CpG ODN C; Lip/Poly(I:C), lipid-based nanoparticles containing Poly(I:C).

* Corresponding author.
E-mail addresses: n.r.rahmani@umcutrecht.nl (N.R. Rahmani), f.jahanmard@gmail.com (F. Jahanmard), hassania@terasaki.org (A. Hassani Najafabadi), jipflapper@hotmail.com (J. Flapper), o.dogan95@gmail.com (O. Dogan), a.khodaei-2@umcutrecht.nl (A. Khodaei), g.storm@uu.nl (G. Storm), michielcroes@gmail.com (M. Croes), m.c.kruyt@umcutrecht.nl (M.C. Kruyt), d.gawlitta@umcutrecht.nl (D. Gawlitta), h.h.weinans@umcutrecht.nl (H. Weinans), e.mastrobattista@uu.nl (E. Mastrobattista), s.aminyavari@umcutrecht.nl (S. Amin Yavari).
[1] Authors contributed equally.

https://doi.org/10.1016/j.ejps.2025.107050
Received 24 October 2024; Received in revised form 27 January 2025; Accepted 21 February 2025
Available online 21 February 2025

Additionally, the dosage of BMP-2 used may potentially mask the immune-stimulatory effect. Lip/CpG ODN C holds potential as a bioactive agent for osteoimmunomodulation, although further *in vivo* demonstration should corroborate the current *in vitro* findings.

1. Introduction

Bone has a remarkable ability to self-heal, but large defects caused by trauma, tumor resection, or degenerative diseases can exceed its natural healing capacity (Gillman et al., 2021). Autograft, or bone harvested from the patient's body, is the gold standard for surgical treatment of bone defects. However, there is limited availability, and involves longer surgical time (Cypher et al., 1996). Biomaterial-based bone substitutes are available options that can provide the structural scaffold needed for bone growth but often lack properties to induce new bone formation (Cypher et al., 1996). Studies report that the immune environment surrounding bone biomaterial can provide the signals needed for the proliferation and differentiation of bone progenitor cells (Chen et al., 2016). Accordingly, recent designs of bone biomaterials involve the incorporation of immunomodulatory properties aiming to enhance bone formation, referred to as osteoimmunomodulation (Chen et al., 2016).

Several studies demonstrate that microbe-derived components can promote new bone formation indirectly via modulation of the immune response (Croes et al., 2019; Croes et al., 2017; Shi et al., 2018). Calcium phosphate-based bone substitutes treated with a combination of bone morphogenetic protein (BMP)−2 and killed bacteria or bacterial components resulted in increased new bone formation compared to BMP-2 alone after implantation at an extra-skeletal location (Croes et al., 2019). It is suggested to involve the activation of pathogen recognition receptors (PRRs) expressed by immune cells. PRRs bind to conserved molecular motifs present in microorganisms, known as pathogen-associated molecular patterns (PAMPs) (Medzhitov, 2007). Activation of PRRs leads to the production of various inflammatory mediators, among which TNF, IL-6, IL-17a, OSM, SDF1-α, and interferons play an important role in the recruitment and differentiation of bone progenitor cells (Croes et al., 2016, 2015; Guihard et al., 2012; Kitaori et al., 2009; Ono et al., 2016; Sims, 2021; Tang et al., 2018). However, it is not yet known what type of microbial-induced immune profile can favor bone formation, since the addition of too-strong stimuli such as active bacteria or bacterial lipopolysaccharide (LPS) inhibits bone formation (Croes et al., 2017).

CpG-containing oligonucleotides type C (CpG ODN C) and Polyinosinic:polycytidylic acid (Poly[I:C]) are analogs of bacterial and viral nucleic acids that have been studied for various immunotherapeutic applications (Ammi et al., 2015). CpG ODN C activates a PRR called toll-like receptor (TLR) 9 and Poly(I:C) activates TLR 3, both receptors are located intracellularly (Alexopoulou et al., 2001; Krieg, 2002; Kato et al., 2006). However, the challenge of employing microbial nucleic acid *in vivo* is the rapid enzyme degradation upon administration and the delivery to reach intracellular receptors (De Temmerman et al., 2011; Hafner et al., 2013). To protect CpG ODN C and Poly(I:C) and facilitate its delivery, we encapsulated each nucleic acid in a lipid-based nanoparticle. Lipid-based nanoparticles are spherical structures with an outer layer formed mainly by phospholipids and an inner core that can carry nucleic acid cargo (Hu et al., 2024). It is biocompatible, biodegradable, and can facilitate the delivery of cargo across the cell membrane (Bozzuto and Molinari, 2015). Once inside the endosome, the lipid-based nanoparticle disrupts releasing its cargo into the cytosol (Albertsen et al., 2022). Depending on their physicochemical properties, lipid-based nanoparticles can be taken up by immune cells (e.g. neutrophil, macrophage, dendritic cells) through endocytosis or phagocytosis (Bozzuto and Molinari, 2015). Therefore, an optimum system to carry CpG ODN C and Poly(I:C).

Most applications that utilize lipid-based nanoparticles are in the form of aqueous solutions since contact with solid surfaces causes rupture (Vermette et al., 2004). We have recently optimized the immobilization of lipid-based nanoparticles on a bone implant surface using a polymeric hydrogel, gelatin methacyrloyl (GelMA) (Jahanmard et al., 2023). GelMA functions as a lyoprotectant and was found to support lipid-based nanoparticles from fusion and aggregation, as well as maintain its intactness under different storage conditions for a prolonged time (Jahanmard et al., 2023). Using GelMA, we can form a stable film containing lipid-based nanoparticle on the surface of implants, maximizing the local therapeutic effects and minimizing off-target or systemic effects.

This research explores the potential of CpG ODN C and Poly(I:C) as an osteoimmunomodulatory agent for bone regenerative purposes. For this, we conducted several experimental processes. First, we encapsulated microbial nucleic acid in a lipid-based nanoparticle to facilitate its delivery into the cytosol of immune cells and as a protective capsule for *in vivo* application. Second, we evaluated the effectiveness of the lipid-based nanoparticles to induce immune cell activation and promote osteoblast differentiation of human mesenchymal stromal cells *in vitro*. Lastly, we coated biphasic calcium phosphate (BCP) bone substitute with bone morphogenetic protein (BMP)-2 and lipid-based nanoparticles suspended in GelMA. The implants were evaluated for *de novo* bone formation in a challenging extra-skeletal (ectopic) implantation model *in vivo*.

2. Materials and methods

2.1. Materials

1,2-dipalmitoyl-sn-glycero-3-phosphocholine (DPPC), 1,2-dipalmitoyl-sn-glycero-3-phospho-(1′-rac-glycerol) (sodium salt) (DPPG), 1,2-dioleoyl-3-dimethylammoniumpropane (DODAP), and L-a-phosphatidylethanolamine-N-(Lissamine Rhodamine B sulfonyl) (Rh-PE) were purchased from Avanti Polar Lipids (USA); and cholesterol (CH) was purchased from Sigma-Aldrich (USA).

Microbial nucleic acid, C-class CpG oligodeoxynucleotide (CpG ODN C, clone M362) and high molecular weight Polyinosinic:polycytidylic acid (Poly[I:C]) were purchased from Invivogen (USA). Concentrated nucleic acid solutions (1 mg/ml) were prepared in endotoxin-free water and stored at −20 °C.

Commercially available biphasic calcium phosphate (BCP) bone substitute (MagnetOs©; Kuros Biosciences BV, The Netherlands) was used as a scaffold in the form of cylindrical discs (9mm Ø; 6 mm height). The BCP comprised of 65–75 % tri-calcium phosphate ($Ca_3(PO_4)_2$) and 25–35 % hydroxyapatite ($Ca_{10}(PO_4)_6(OH)_2$) with a submicron needle-shaped surface topography (Van Dijk et al., 2019). BCPs were sterilized by autoclaving at 121 °C for 30 min and drying at 60 °C.

2.2. Lipid-based nanoparticle synthesis and characterization

Lipid-based nanoparticles were synthesized using an ethanol dilution method (Jeffs et al., 2005). First, lipids (DPPC, DODAP, CH, and DPPG) were dissolved in 90 % (v/v) ethanol with a total lipid concentration of 20 mM and a molar ratio of 38/25/30/7, respectively. The lipid ethanol mixture was heated in a water bath (50 °C) and mixed vigorously using a vortex mixer to ensure dissolution. Separately, nucleic acid solutions were prepared by mixing nucleic acid stock (1 mg/ml of CpG ODN C or Poly[I:C]) with citrate buffer (67 mM, pH 4.0) and distilled deionized water, arriving at a final condition of 200 ug/ml nucleic acid and 40 mM citrate buffer. Then, using a 1 ml sterile plastic syringe and needle (0.45×22 mm), the lipid-ethanol mixture (500 μl) was added dropwise

into the nucleic acid solution (500 μl) in a glass vial under continuous agitation with a magnetic stirrer at room temperature. The solution was diluted by adding (dropwise) an equal volume of 20 mM citrate buffer (pH 4.0) containing 300 mM NaCl, then left to stand for 1 hour at room temperature to facilitate vesicle formation. Ethanol was removed by dialysis (cassette MWCO 10 kDa Slide-A-Lyzer G2, Life Technologies, USA) against 20 mM citrate buffer (pH 4.0) containing 150 mM NaCl for 2 h at 4 °C (refreshed completely each hour), followed by overnight dialysis in HEPES buffer saline (HBS, pH 7.4) at 4 °C to neutralize DODAP. All dialysis buffers were 1000x more than the sample volume. Non-encapsulated nucleic acids were removed by 3 rounds of ultracentrifugation (Type 70.1 Ti rotor) at 55,000 RPM for 50 min at 4 °C. The supernatant was removed and the lipid-based nanoparticles were resuspended in HBS to achieve a theoretical lipid concentration of 30 mM, then stored at 4 °C until use.

The hydrodynamic diameter and polydispersity index (PDI) of the lipid-based nanoparticles were measured using dynamic light scattering (Nano-S, Malvern, UK) with a detection angle of 173° (backscatter) at 25 °C following a 2-minute incubation. Zeta potential was measured using laser Doppler electrophoresis (Zetasizer Nano-Z, Malvern, UK) under the same conditions. For both measurements, nanoparticles were dispersed at 2.5 % v/v in a low ionic buffer (10 mM HBS, pH 7.4) in triplicate. The hydrodynamic diameter and PDI measurements utilized semi-micro polystyrene cuvettes (Sarstedt, Germany) with a 10 mm path length and 3 ml maximum working volume, while zeta potential measurements employed PCS1115 cuvettes (Malvern, UK), which are 12 mm square glass cells compatible with all Nano series systems designed for zeta potential measurements.

Lipid-based nanoparticles were suspended in gelatin metacryloyl (GelMA, see Section 2.4) and applied on Formvar-coated grids for transmission electron microscopy (TEM) (FEI Tecnai 12, Thermosystems, USA) to visualize structure. While it's distribution in GelMA suspension was visualized by confocal microscopy (Leica SP8X, Germany). To aid visualization of lipid-based nanoparticles, Rh-PE (40 μg/ml), a fluorescent dye, was added into the lipid ethanol mixture during synthesis.

2.3. Encapsulation and loading efficiency

Encapsulation and loading efficiency were calculated based on direct measurements of the amount of CpG ODN C or Poly(I:C) encapsulated in lipid-based nanoparticles. As described in Section 2.2 the final lipid nanoparticle solutions have been removed from non-encapsulated nucleic acids. Thereafter, the lipid and nucleic acid components were separated using the lipid extraction method (Bligh and Dyer, 1959) resulting in a top phase containing nucleic acid and a bottom phase containing lipids. Both phases were dried using a vacuum concentration, then the nucleic acid component was reconstituted in Mili-Q water while the lipids with 2:1 chloroform mixture. The nucleic acid content was measured using the Quant-iT™ PicoGreen™ dsDNA kit assay for CpG ODN C and the Quant-it™ RiboGreen RNA kit assay for Poly(I:C) (Invitrogen, Thermo Fischer Scientific), following the respective manufacturer's protocols. The lipid contents (phospholipids DPPC and DPPG) were measured using the Rouser method (Rouser et al., 1970), with sodium biphosphate as the internal standard. The encapsulation efficiency and loading efficiency were calculated with the following formulations:

$$\text{Encapsulation efficiency (\%)} = \frac{\textit{Encapsulated nucleic acid (mass)}}{\textit{initial nucleic acid (mass)}} \times 100$$

$$\text{Loading efficiency } (\mu g \,/\, \text{mmol lipid}) = \frac{\textit{initial nucleic acid } (\mu g) \textit{ x Encapsulation efficiency (\%)}}{\textit{total lipid (mmol) x Lipid recovery (\%)}}$$

2.4. Gelatin methacryloyl (GelMA) synthesis

GelMA was synthesized as previously described (Jahanmard et al., 2023; Müller et al., 2020). Briefly, porcine gelatin type A (~175 g Bloom, G2625, Sigma-Aldrich) 10 % w/v was dissolved in PBS at 50 °C with continuous agitation for 1h. Methacrylic anhydride (276685, Sigma-Aldrich) 60 % w/v was added dropwise to the stirring solution. A 3x volume of PBS was added and the pH was adjusted to 7.4 with 5 mM NaOH. Excess of methacrylic anhydride was removed by centrifugation and subsequently dialyzed (cellulose membrane with 12–14 kDa cut off, Sigma Aldrich) in deionized water at 4 °C for 5 days. The solution was filtered through a 0.22 μm membrane, lyophilized, and stored in a sealed container at −20 °C until further use.

2.5. Implant preparation

Implants consisted of a BCP scaffold, low-dose BMP-2, and a hydrogel containing nucleic acids. First, GelMA/irgacure mixture (9 %/0.75 % wt% in HBS) was prepared. Irgacure functions as a photoinitiator which will facilitate the crosslinking of GelMA when exposed to UV light (Van Den Bulcke et al., 2000). Irgacure (410896, Sigma-Aldrich, USA) was dissolved by heating to 60 °C and stirred until dissolved. Lyophilized GelMA was added to the solution and vortexed firmly until dissolved. The mixture was filtered through a 0.45 μm syringe filter. The mixture was kept in the dark and left cooled to room temperature. Afterward, nucleic acid (100 μg/ml) diluted in HBS was added to the mixture. Separately, recombinant human BMP-2 (100 μg/ml, InductOS®, Wyeth/Pfizer, USA) in PBS was prepared.

BCP discs were placed on a sterile plate. 50 μl of BMP-2 was pipetted evenly onto the disk followed by 150 μl of GelMa/Irgacure/nucleic acid mixture. BCP retained the total volume of 200 μl without leaks. The final conditions of each implant were BMP-2 25 μg/ml, GelMA 6 % wt%, irgacure 0.5 % wt%, and nucleic acid 1 μg/ml. The concentration of BMP-2 was chosen based on a pilot *in vivo* study (Suppl. Fig. A.1). Subsequently, the implant was exposed to UV light (Bluepoint Ecocure, Germany) for 3 mins on each side to crosslink GelMA forming a solidified hydrogel coat on the BCP.

Six groups of implants were prepared, one control and 5 experimental groups. The control group ($n = 24$), implanted in each animal, consisted of BMP-2 + empty GelMA. The experimental groups (each $n = 8$) consisted of BMP-2 and GelMA containing nucleic acids: Poly(I:C), CpG ODN C, Lip/Poly(I:C), and Lip/CpG ODN C; and 1 group consisted of BMP-2 + GelMA containing empty lipid-based nanoparticles (Lip). All implants were prepared one week before surgery and stored in a sealed compartment at 4 °C until use. Preparations were done under sterile conditions.

2.6. Visualization of GelMA distribution on BCP discs

GelMA was mixed with a dye to visualize its distribution on BCP discs. First, GelMA/irgacure mixture was prepared as described in Section 2.5. Then fluorescein isothiocyanate-dextran (FITC, FD70S, Sigma Aldrich) dye 1 % v/v was added to the mixture and vortexed until homogenous. PBS (50 μl) was pipetted onto a BCP disc, followed by GelMA/irgacure/FITC mixture (150 μl). The implant was placed under UV light for 3 mins on each side to crosslink GelMA. Subsequently, the implant was washed in PBS, fixed in 4 % formaldehyde, washed in Milli-Q, and left to air-dry overnight. Images were taken with a stereomicroscope and scanning electron microscope (SEM, 5Kv, 60 Pa). Before SEM imaging, the implant was coated with 8 nm of gold to increase conductivity.

2.7. Release of lipid-based nanoparticles from the implants and GelMA degradation rate

The release of lipid-based nanoparticles from the implants and the degradation rate of GelMA were measured over time. Three groups of implants were prepared (in triplicates): Lip/CpG ODN C, Lip/Poly(I:C, and Lip (empty/no cargo). Implants were immersed in 1 ml PBS and placed in an incubator at 37 °C. Medium were collected and refreshed daily for 7 days and on day 14. The lipid-based nanoparticles released in the media were measured by separating the lipid components from the nucleic acids as described in Section 2.3. Measurement of the lipid contents, rather than the nucleic acid, was used as a parameter to compare the release profile between implants. To determine the cumulative release curves, the lipid measured from the medium was normalized to the total drug content.

For measurement of GelMA degradation, 4 groups of implants (in triplicates) were prepared: GelMA/Lip, GelMA/BMP-2, GelMA/BMP-2/Lip, and empty GelMA. Implants were immersed in 1 ml PBS and placed in an incubator at 37 °C. Medium were collected and then refreshed after 1 h, 6 h, and then daily for 7 days. GelMA released in the medium was measured indirectly using the bicinchoninic acid (BCA) protein assay kit (Thermo Fisher, USA).

2.8. Liposome uptake

RAW 264.7 macrophages were seeded at a density of 155,000 cells/cm^2 in medium consisting of RPMI (Gibco, Thermo Fisher, USA) supplemented with 10 % (v/v) heat-inactivated FBS, 100 U/mL penicillin and 100 μg/mL streptomycin. Cells were incubated overnight with Lip, Lip/CpG ODN C, and Lip/Poly(I:C) all containing Rh-PE (40 μg/ml) fluorescent dye. Cell nuclei were stained with DAPI (2 μg/ml, Abcam, UK) for 30 min, then intact lipid-based nanoparticles were detected by confocal microscopy.

2.9. Cytotoxicity assay

Primary human mesenchymal stromal cells (MSCs) were seeded at a density of 15,000 cells/cm^2 and cultured in minimum essential medium (α-MEM, Gibco, Thermo Fisher, USA) supplemented with 10 % (v/v) heat-inactivated FBS, 100 U/ml penicillin and 100 U/ml streptomycin, 0.2 mM L-ascorbic acid-2-phosphate (Sigma-Aldrich, USA). Cells were stimulated with CpG ODN C, Poly(I:C), Lip/CpG ODN C, Lip/Poly(I:C), or Lip (at 0.1; 1; 10 μg/ml); and with the released medium of day 1–3 from the different implant groups (implant preparation in Section 2.5). For this experiment, BMP-2 was not included in the implants. Unstimulated cells were used as control.

At days 1 and 4, MSCs metabolic activity was measured by adding 10 % of Alamar Blue Cell Viability Reagent (Thermo Scientific, US) into the culture medium. After a 3-hour incubation, fluorescence was measured at 544/590 nm using a plate reader (Fluoroskan Ascent FL multi-plate reader, Thermo Labsystems, Finland).

2.10. Immunostimulatory assay

Macrophages were derived from primary human monocytes. Briefly, peripheral blood was obtained from 3 healthy donors (Mini Donor Dienst, University Medical Center Utrecht, The Netherlands). The mononuclear fraction was separated by gradient density as previously described (Khokhani et al., 2022). Then CD14+ monocytes were purified by magnetic-activated cell sorting (MACS®) separation protocol using CD14 micro beads (cat. 130–050–201, Miltenyi Biotec, USA). Monocytes were cultured in RPMI 1640 medium supplemented with 10 % (v/v) heat-inactivated FBS, 100 U/mL penicillin and 100 μg/mL streptomycin, and 25 ng/ml of Macrophage Colony Stimulating Factor (M-CSF, 300–25, Peprotech, USA) for 7 days to induce macrophage differentiation.

Macrophages (3 donors, each in triplicates) were stimulated for 24 h with CpG ODN C, Poly(I:C), Lip/CpG ODN C, Lip/Poly(I:C), or Lip (at 0.1; 1; 10 μg/ml). Lipopolysaccharide (100 ng/ml, LPS, 055:B5, Sigma-Aldrich, USA) was included as a positive control. Conditioned media were collected and measured for cytokines: tumor necrosis factor (TNF), interleukin (IL) 6, IL-8, and IL-10 levels using enzyme-linked immunosorbent assays (R&D Systems® DuoSet ELISA Kits). A part of the conditioned medium was also stored at −20 °C to be used for the osteoblast differentiation assay (Section 2.11.).

2.11. Effect of microbial nucleic acids on osteoblast differentiation in vitro

MSCs were seeded at a density of 15,000 cells/cm^2 and cultured in osteogenic differentiation medium (ODM) consisting of α-MEM supplemented with 10 % (v/v) heat-inactivated FBS, 100 U/mL penicillin and 100 μg/mL streptomycin, 0.2 mM L-ascorbic acid-2-phosphate, 10 mM β-glycerophosphate (Sigma-Aldrich, USA) and 10 nM dexamethasone (Sigma-Aldrich, USA) (Pennings et al., 2019).

To study the direct effect of microbial nucleic acids on osteoblast differentiation, MSCs were exposed with CpG ODN C, Poly(I:C), Lip/CpG ODN C, Lip/Poly(I:C), or Lip (at 0.1; 1; 10 μg/ml). To study immune-mediated effects on osteoblast differentiation, MSCs were exposed to the conditioned medium collected from stimulated macrophage (see Section 2.10). The ratio of osteogenic medium and macrophage-conditioned medium was 1:8. In all settings, MSCs were exposed to the various conditions in the first 2 days of culture, after which the medium was replaced with plain ODM.

Alkaline phosphatase activity as an indicator of early osteoblast differentiation was measured on day 4 and 10. Briefly, cells were lysed with 0.2 % (v/v) Triton-X 100/PBS for 30 minutes. ALP activity was determined by the hydrolysis reaction of p-nitrophenyl phosphate liquid substrate system (pH 9.6) (SIGMA*FAST*™ pNPP tablets; Sigma-Aldrich, USA). Absorbance was measured at 405 nm and corrected at 655 nm (Bio-Rad, Hercules, USA). ALP activity values were normalized to total DNA content, measured with the Quant-It PicoGreen kit.

2.12. Animal experiments

Intramuscular ectopic implantations were performed on 24 New Zealand white rabbits (female, 20–25 weeks old, 3–4 kg, Crl:KBL, Charles River, France). All procedures were performed following the EU Directive 2010/63/EU for animal experiments and approved by the national animal ethics committee (AVD1150002016445). Food and water were provided *ad libitum* and animal's general well-being were checked daily. Animals received also implants at other locations for different studies to comply with the 3Rs' principle of reduction (Rahmani et al., 2024)

Animals received a prophylactic antibiotic with Penicillin (4×10^4 mg/kg s.c., Duplocilline®, Merck Animal Health, USA). General anesthesia was induced by Etomidat (1.8 mg/kg i.v) and maintained with Sufentanyl (0.037 mg/kg) and Isofluorane (2–2.5 ml/hour). The dorsal

skin was shaved and disinfected with povidone-iodine. The paraspinal muscles were exposed through a midline incision (±7 cm). Three intramuscular pockets were made by small incisions (±1 cm) with 4 cm between the pockets. Each animal received one control implant and two experimental implants (see Section 2.5 for experimental groups). The type of experimental group and location of implantation followed a randomization list generated online. Incisions were closed layer by layer with absorbable sutures (4.0 Monocryl®, Ethicon, USA). Buprenorphine (0.03 mg/kg s.c.; Temgesic®, Belgium) was given as pain medication.

The animal received calcein green injection (10 mg/kg s.c. in 0.2 M $NaHCO_3$, Sigma-Aldrich, USA) at 2 weeks and xylenol orange injection (30 mg/kg s.c. in 0.12 M $NaHCO_3$, Sigma-Aldrich, USA) at 3 weeks after surgery, to evaluate the onset of bone formation. At week 5, euthanasia was induced by overdose of pentobarbital (Euthanimal®, Alfasan Nederland BV, The Netherlands). Implants were harvested and fixed in 4 % formaldehyde. A quarter of each implant was cut with a circular saw (Dremel 4000, Mount Prospect, USA) to be decalcified (in 0.5 M EDTA) and embedded in paraffin. The remaining three-quarters of the implant was processed for embedding in methyl methacrylate (MMA, Merck Millipore, USA).

2.13. Bone histomorphometry and fluorochrome detection

Implants were dehydrated in an ethanol series of 70 %, 96 %, and 100 % ethanol for 1–2 days per step. After dehydration, implants were immersed in a mixture of MMA with 20 % (v/v) plastoid N (Sigma-Aldrich, United States) and 2.8 % (w/v) benzoyl peroxide (Luperox, Sigma-Aldrich, United States). Implants were placed in a water bath at 37°C for 3 h to start polymerization.

Four think slices (±30 μm) were made on the middle third region of the implants using a saw microtome (Leica, Nußloch, Germany). Two slices were stained with basic fuchsin and methylene blue, and the remaining two were left unstained. Stained slices were pseudo-colored using Adobe Photoshop 2020 (Adobe Systems, USA) to distinguish scaffold and bone tissue. Bone volume within the pore areas was quantified by calculating the proportion of bone pixels relative to the total pore area (expressed as bone area %). Scaffold degradation (%) was quantified by calculating the proportion of scaffold pixels relative to the reference. The reference was the average scaffold pixel obtained from 4 non-implanted BCPs.

Fluorochrome signals were detected from unstained slices using a laser scanning confocal microscope to detect calcein green (494/509–550 nm), xylenol orange (570/610–780 nm) and white light laser (470–670 nm).

2.14. Histological characteristics

A quarter of each implant was decalcified in 0.5 M EDTA for 3–4 weeks, before embedded in paraffin. Samples were sectioned, dewaxed, and stained with Hematoxylin and eosin for routine examination. Osteoclasts were detected with staining for tartrate-resistant acid phosphatase (TRAP) activity. Briefly, samples were incubated in 0.2 M acetate buffer-tartaric acid (pH 5.0) for 20 min at room temperature. Subsequently, samples were immersed in a fresh solution of Naphtol AS-MX phosphate (0.5 mg/ml, Sigma-Aldrich, United States) and Fast Red TR salt (1.1 mg/ml, Sigma-Aldrich, United States) diluted in 0.2 M acetate buffer-tartaric acid (pH 5.0) for 1.5–2 h at 37°C. Then rinsed and counterstained with Mayer's hematoxylin.

2.15. Statistical analysis

Sample size calculation for the animal experiment was performed with bone volume (area%) as the main outcome parameter. Using an effect size of 50 %, standard deviation of 30 % (Croes et al., 2019), a power of 80 %, and an adjusted alpha of 0.1 %, a sample size of 7 was required. All results are shown as the mean ± standard deviation. Statistical analyses were performed with GraphPad Prism 9 software. The Shapiro-Wilk test was used to determine normality of the data. One-way ANOVA with Tukey's post-hoc test was used for parametric data and Kruskal Wallis for non-parametric data. P values of 0.05 were considered statistically significant.

3. Results

3.1. Physicochemical characteristics of liposome formulations

The ethanol dilution method (Jeffs et al., 2005) was used to formulate the lipid-based nanoparticles. Empty lipid-based nanoparticles (Lip) had an average diameter of 251±3 nm and PDI of 0.05±0.03 (Table 1, Fig. 1A). Lipid-based nanoparticles containing CpG ODN C (Lip/CpG ODN C) had an average diameter of 259±5 nm and PDI of 0.15±0.05. Lipid-based nanoparticles containing Poly(I:C) (Lip/ Poly[I:C]) had an average diameter of 253±3 nm and PDI of 0.19±0.04. Encapsulation efficiency by direct measurement of nucleic acid content was ±60 % (Table 1). The zeta potential was in the range of −36 to −40 mV (Table 1, Fig. 1B). Visualization of lipid-based nanoparticles transmission electron microscopy revealed vesicles with single to multiple bilayer(s) (Fig. 1C).

To prepare implants for *in vivo* application, lipid-based nanoparticles were suspended in gelatin methacryloyl (GelMA) hydrogel to preserve its intactness (Jahanmard et al., 2023). Visualization of Lip suspension in GelMA showed a uniform distribution with no cluster formation (Fig. 1E).

3.2. Release of lipid-based nanoparticles from the implant and GelMA degradation rate

Implants were prepared for *in vivo* application. It consisted of a BCP scaffold, BMP-2, and a GelMA hydrogel containing microbial nucleic acids in their free form or encapsulated in lipid-based nanoparticles (Fig. 2A). GelMA was mixed with a dye to visualize its distribution of BCP scaffold. From a macroscopic view (Fig. 2B), GelMA is shown to be distributed mainly on the outer surface of the BCP and also seen in the pores (crossectional view). Microscopic view using electron microscopy shows GelMA on the surface of the BCP and in between the needle-shaped crystals (Fig. 2C).

The release of lipid-based nanoparticles from the implants was measured (Fig. 2D). At day 1, 75 % of Lip/Poly(I:C) was released from the implants. Lip/CpG ODN C displayed a slower release pattern, with about 30 % by day 1, followed by a gradual release of 5–10 % up to day 7. Lastly, approximately 60 % of Lip was released by day 1. The degradation profile of GelMA was similar for all cases, with

Table 1
Physicochemical characteristics of the liposome formulations.

	Mean size (nm)	PDI	Zeta potential (mV)	Lipid recovery (%)	Encapsulation efficiency (%)	Loading efficiency (μg/mmol lipid)
Lip (empty)	251±3	0.05±0.03	−36±2	48±1	–	–
Lip/CpG ODN C	259±5	0.15±0.05	−37±3	43±5	60±1	28
Lip/Poly (I:C)	253±3	0.19±0.04	−40±2	52±3	61±3	23.5

Values are presented as mean±SD ($n = 3$). PDI = polydispersity index.

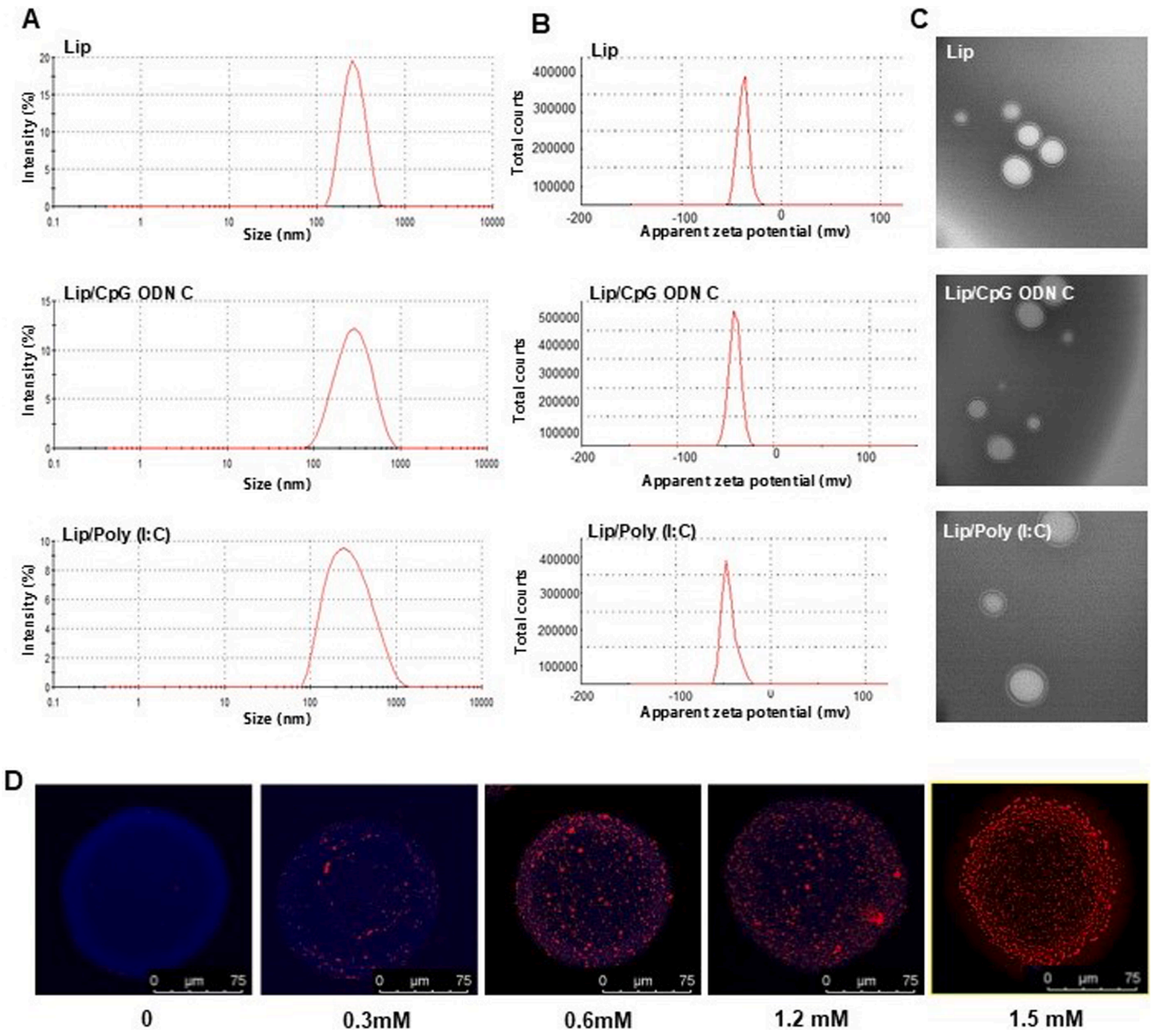

Fig. 1. Characterization of lipid-based nanoparticles. **(A)** Size distribution of lipid-based nanoparticles by intensity and **(B)** zeta potential. **(C)** Transmission electron microscopic (TEM) images showing lipid-based nanoparticles as spherical vesicles with single to multiple bilayer(s). **(D)** Distribution of intact Lip (red, 0–1.5 mM) suspended within a GelMA microsphere (blue), visualized by fluorescence confocal microscopy.

approximately 40 % degraded at the first hour, 60 % at 6 h, and 80 % at 24 h (Fig. 2E). Complete degradation of GelMA occurred in 7 days.

3.3. *Increased macrophage stimulation by nucleic acids encapsulated in lipid-based nanoparticles*

We first assessed whether lipid-based nanoparticles affected cell viability in culture. MSCs were exposed to different concentrations of Lip/CpG ODN C, Lip/Poly(I:C), and Lip directly or exposed with the released medium of day 1–3 from the different implant groups. No noticeable impact was seen on MSCs' metabolic activity after 1 and 4 days (Fig. 3A). Visualization by confocal microscopy confirmed that lipid-based nanoparticles were taken up by macrophages and clustered in the cytoplasm (Fig. 3B).

The immunostimulatory assay showed that CpG ODN C and Poly(I:C) by themselves induced similar levels of cytokine secretion with non-stimulated macrophages (Fig. 3C). Meanwhile, Lip/CpG ODN C increased IL-6 secretion and Lip/Poly(I:C) increased TNF, IL-6, and IL-10 secretion. This suggests stronger macrophage activation by the nucleic acids when carried in a lipid-based nanoparticle. Interestingly, Lip (empty cargo) by itself induced a higher trend of TNF, IL-6, and IL-10 secretion compared to non-stimulated macrophages. IL-8 levels were comparable between groups. The cytokines tested here are general indicators of immune cell activation and are not specific parameters for TLR3 or TLR9 activation, the receptors of Poly(I:C) and CpG ODN C, respectively. For data on the immunostimulatory assay for all concentrations see Suppl. Fig. A2.

3.4. *Lip/CpG ODN C performed better than CpG ODN C to promote osteoblast differentiation through immune-mediated effects*

Osteoblast differentiation of MSCs was not affected by the direct exposure to CpG ODN C, Poly(I:C), Lip/CpG ODN C, Lip/Poly(I:C), or Lip (Fig. 3D). However, ALP activity, as indicator of early osteoblast differentiation, increased when MSCs were exposed to the conditioned medium collected from macrophages stimulated with 10 μg/ml CpG

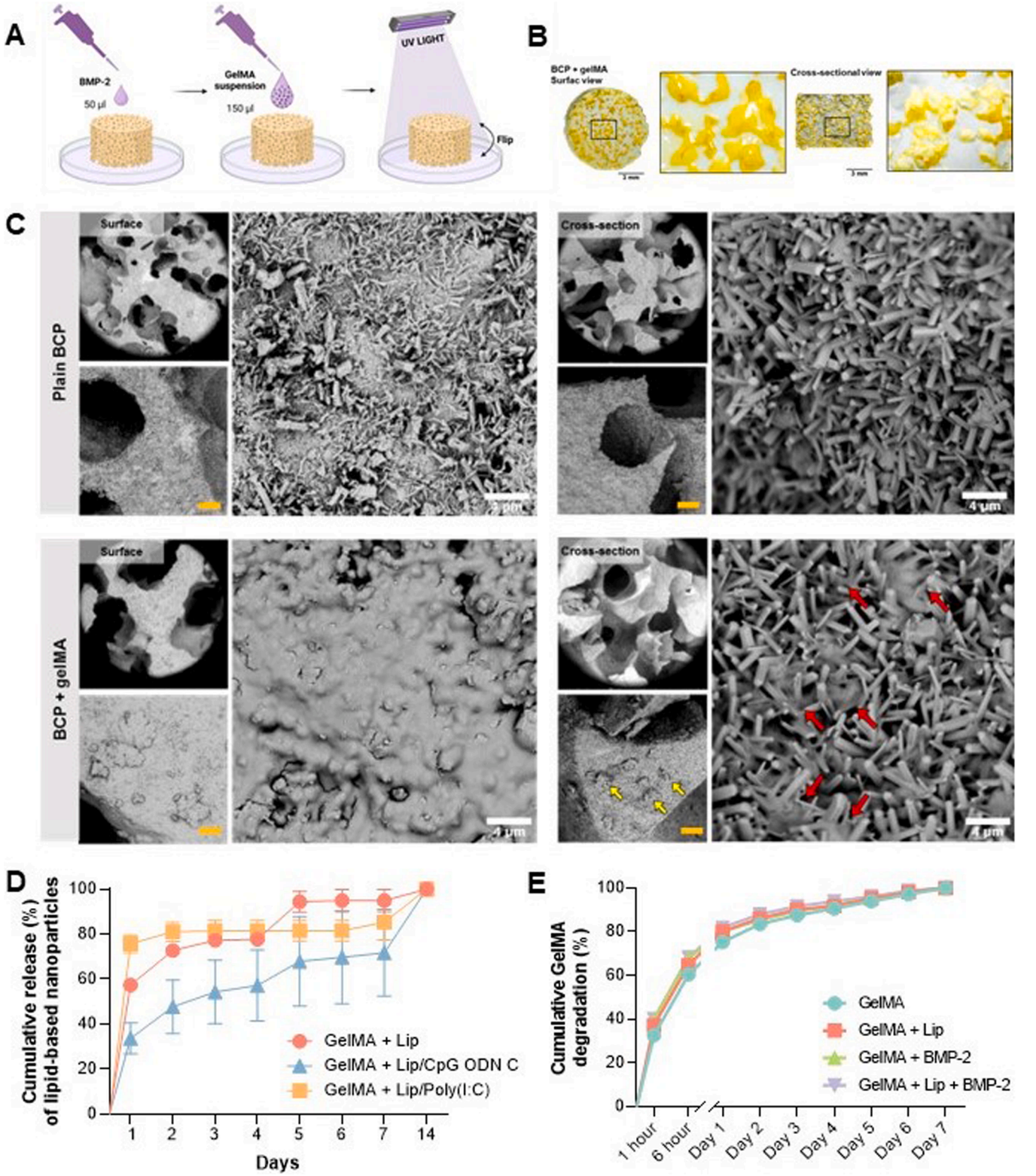

Fig. 2. Characterization of the implants. **(A)** Implant preparation scheme. BMP-2 was pipetted onto BCP scaffold, followed by GelMA suspension containing lipid-based nanoparticles, and then placed under UV light to solidify GelMA. **(B)** Macroscopic view of GelMA distribution (stained yellow) on BCP disc after crosslinking. **(C)** Scanning electron microscope (SEM) images of plain BCP and BCP+GelMA. GelMA is seen to cover the surface of the BCP shown by a smooth appearance. Cross-sectional view depicts sparsely distributed GelMA in the pores (yellow arrows) and in between the needle-shaped crystals (red arrows). **(D)** Cumulative release of lipid-based nanoparticles from the implants. **(E)** Cumulative degradation of GelMA in the implants.

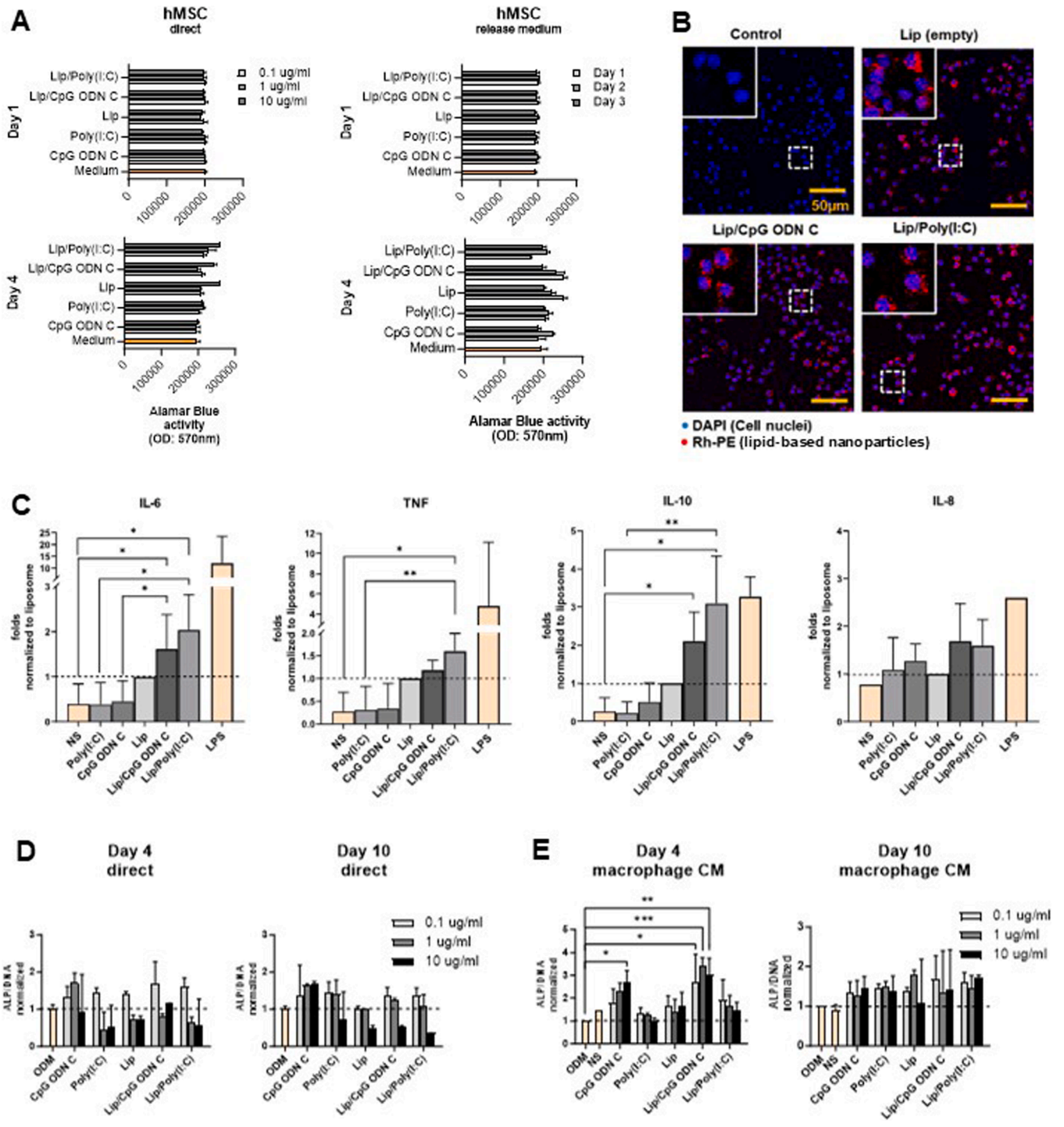

Fig. 3. *In vitro* assays for osteoimmunomodulatory properties. **(A)** Metabolic activity in cell culture measured by alamar blue activity at days 1 and 4 of hMSCs stimulated directly with CpG ODN C, Poly(I:C), Lip/CpG ODN C, Lip/Poly(I:C), or Lip (at 0.1; 1; 10 μg/ml); or with the released medium of day 1–3 from the different implant groups. For this assay, implants did not contain BMP-2. **(B)** Lipid-based nanoparticles (red, containing Rh-PE fluorescent dye) visualized inside the cytoplasm of murine macrophages (nuclei stained blue) after 24h. Inserts depict 3x magnification **(C)** IL-6, TNF, IL-10, and IL-8 cytokine secretion levels of primary human macrophages stimulated with 1 μg/ml of CpG ODN C, Poly(I:C), Lip/CpG ODN C, Lip/Poly(I:C), or Lip. LPS (100 ng/ml) was used as a positive control. Data is normalized to Lip and depicted as mean±SD from 3 donors in triplicates. **(D)** Alkaline phosphatase (ALP) activity/DNA measured at days 4 and 10 of hMSCs exposed to CpG ODN C, Poly(I:C), Lip/CpG ODN C, Lip/Poly(I:C), or Lip (at 0.1; 1; 10 μg/ml) during osteogenic differentiation. Data is normalized to osteogenic medium (ODM) and depicted as mean±SD from one MSC donor in triplicates. **(E)** ALP activity/DNA measured at days 4 and 10 of hMSCs exposed to the conditioned medium (CM) of macrophages stimulated with CpG ODN C, Poly(I:C), Lip/CpG ODN C, Lip/Poly(I:C), or Lip (at 0.1; 1; 10 μg/ml). Data is normalized to ODM and depicted as mean±SD from 1 MSC donor and 2 macrophage donors in triplicates. NS = non-stimulated macrophages. $*P < 0.05$ / $**P < 0.005$/ $***P < 0.001$.

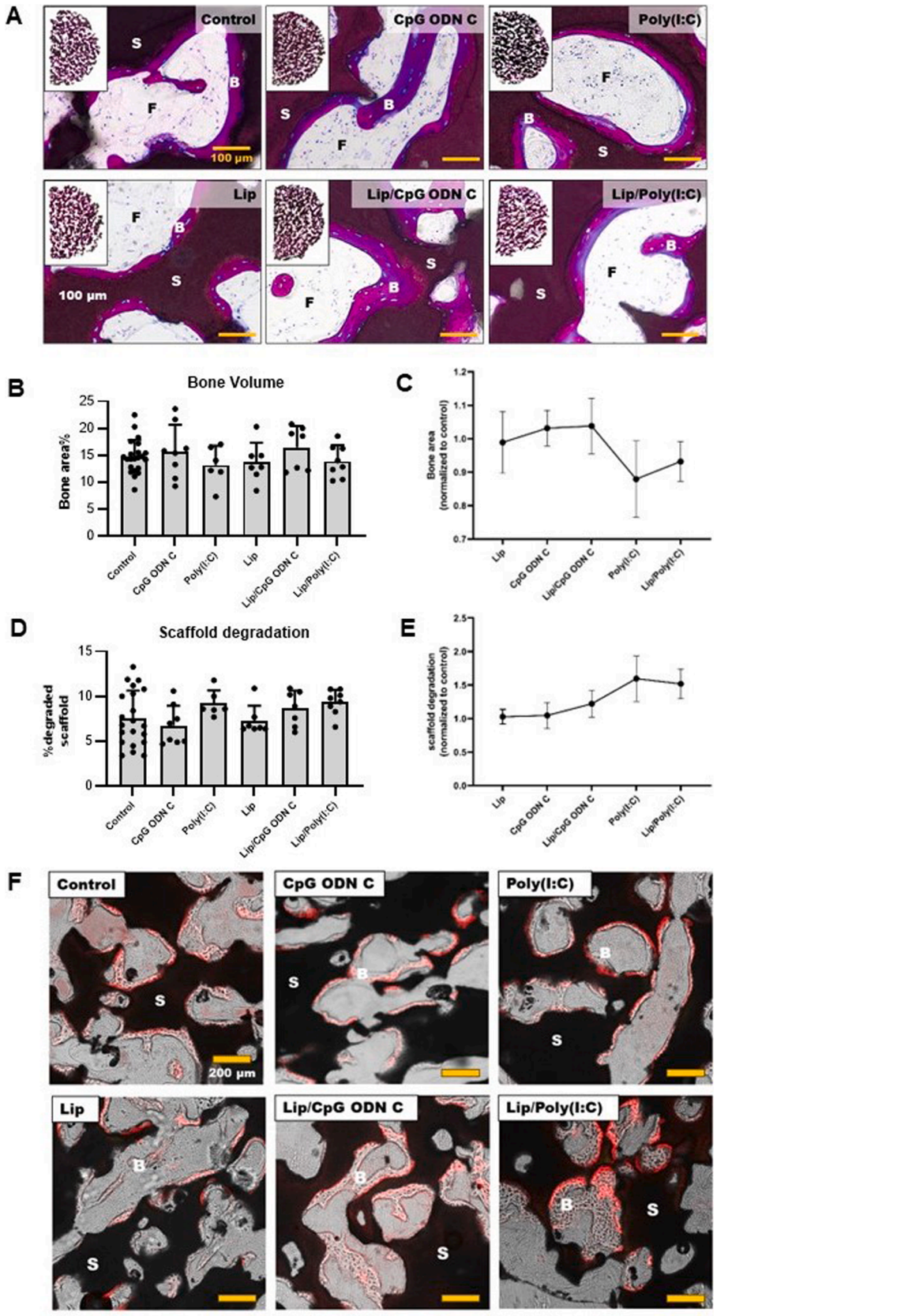

(caption on next page)

Fig. 4. Histomorphometric analysis of new bone formation in implants placed inside intramuscular pockets of rabbits after 5 weeks. **(A)** Basic fuchsin and methylene blue staining showing bone (B, pink), scaffold (S, dark brown), and fibrous tissue (F). Insert depicts the distribution of bone in the implant. **(B)** Average bone volume (area%) of the control group (empty GelMA, $n = 24$) and experimental groups ($n = 8$). All implants contained BMP-2 (5 μg). Data are presented as mean±SD. **(C)** Fold changes in bone volume of each experimental implant relative to its respective control, implanted in the same animal (normalized to the corresponding control). Data are presented as mean±SD. **(D)** Average scaffold degradation (%) of the control group (empty GelMA, $n = 24$) and experimental groups ($n = 8$). Data are presented as mean±SD. **(E)** Fold changes in scaffold degradation of each experimental implant relative to its respective control, implanted in the same animal (normalized to the corresponding control). Data are presented as mean±SD. **(F)** Positive signal for xylenol orange (red) fluorescent label administered 3 weeks of after implantation is detected; B=bone, S=scaffold.

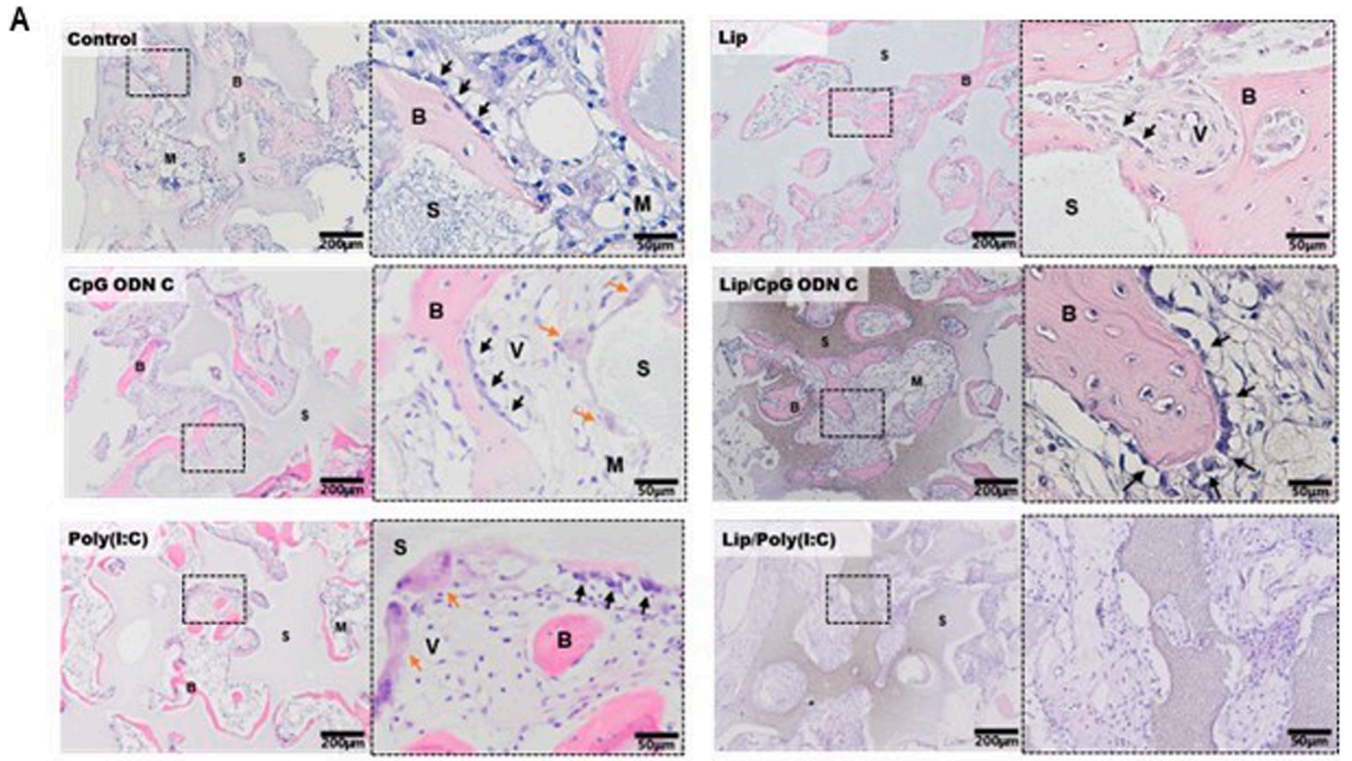

Fig. 5. Histological characteristics of implants after 5-weeks implantation. **(A)** Bone tissue stained with haematoxylin and eosin stain showing the presence of osteoblast (black arrow), bone (B), blood vessels (V), and marrow-like tissue (M), within the pores of the scaffold (S). **(B)** Distribution of TRAP-positive multinucleated cells (red), scale bar = 200μm.

ODN C (2.6-fold) and with 0.1, 1, and 10 μg/ml of Lip/CpG ODN C (3-fold) (Fig. 3E). No effect on osteoblast differentiation was seen for Poly (I:C), Lip/Poly(I:C), or Lip.

3.5. Evaluation of implants on ectopic bone formation in vivo

To determine *de novo* bone formation, implants were evaluated in a challenging extra-skeletal (ectopic) implantation model. Here, implants were placed intramuscularly with no contact with native bone tissue for a period of 5 weeks.

Histomorphometric analysis showed layers of bone tissue in the pores of the implants in direct contact with BCP surface (Fig. 4A). The average bone volume in the control group (BMP-2+empty GelMA) was 14.7 ± 3.1 % (Fig. 4B). Average bone volume in the experimental groups were : Poly(I:C) 13±3.5 %, CpG ODN C 15.7 ± 5 % Lip/Poly(I:C) 13.9 ± 3 %, Lip/CpG ODN C 16.4 ± 4 %, and Lip 13.6 ± 3.6 % (Fig. 4B). Given interindividual variations, we compared the bone volume of each experimental implant with its respective control implanted in the same animal (Fig. 4C). No differences in bone volume were seen between the experimental group and control. The average scaffold degradation in the control group was 7.5 %±3 % (Fig 4D). The average scaffold degradation in the experimental groups were : Poly(I:C) 9.2 ± 1.5 %, CpG ODN C 6.7 ± 2.2 %, Lip/Poly(I:C) 9.3 ± 1.4 %, Lip/CpG ODN C 8.6 ± 1.9 %, and Lip 7.2 ± 1.7 % (Fig. 4D). We compared the scaffold degradation of each experimental implant with its respective control implanted in the same animal (Fig. 4E). No differences in scaffold degradation were seen between the experimental group and control.

To determine the start of mineralization in the newly formed bone, we administered fluorescent dye at weeks 2 and 3 after implantation. We found no fluorescent signal at week 2 and positive signals at week three in all implants (Fig 4F). This indicates that the mineralization onset started 3 weeks after implantation for all groups.

Hematoxylin and eosin staining show fibrous tissue forming inside BCP pores and some layers of bone tissue (Fig. 5A). The implants were well-vascularized with some marrow-like structure. Osteoblasts were found to line the surface of the osteoid suggesting active bone matrix deposition to continue after 5 weeks of implantation. Osteoclasts were present mainly on the BCP surface, suggesting active degradation of the BCP (Fig. 5B). No noticeable differences in the tissue were observed between the experimental groups and control.

4. Discussion

CpG ODN C and Poly(I:C) are analogs of microbial nucleic acids that have been studied for various immunotherapeutic applications. Here we study the potential of CpG ODN C and Poly(I:C) as an osteoimmunomodulatory agent for bone regenerative purposes. CpG ODN C and Poly (I:C) were each encapsulated in a lipid-based nanoparticle and evaluated for osteoimmunomodulatory properties *in vitro* and *in vivo*.

4.1. Formulation of lipid-based nanoparticles

The lipid-based nanoparticles were comprised of DPPC phospholipid and cholesterol which form the outer layers and provide structural stability. DODAP was used as an ionizable cationic lipid, that is deprotonated at neutral pH and positively charged in acidic environments (Albertsen et al., 2022). During assembly of the nanoparticles, the positively charged DODAP interacts electrostatically with the negatively charged CpG ODN C or Poly(I:C). Additionally, DPPG, a helper anionic phospholipid, interacts electrostatically with DODAP, promoting the incorporation of microbial nucleic acids into the nanoparticle core. DPPG contributes to the overall negative charge of the nanoparticles, creating a repulsion force that prevents aggregation in aqueous solutions and improve stability.

The lipid-based nanoparticles are ±250 nm, which is adequate for immune cell uptake through phagocytosis or macropinocytosis (Kay, 2021; Lim and Gleeson, 2011). A proposed mechanism of cargo release from lipid-based nanoparticles is that after cellular uptake, nanoparticles reside in the endosome, then as the endosome matures, the pH decreases causing the ionizable lipid (e.g., DODAP) to be protonated. he net interaction between the positively charged lipid and the negatively charged endosomal membrane will cause the nanoparticle structure to disrupt (Semple et al., 2010). Thereby, releasing cargo into the cytosol enabling the activation of their respective receptors; TLR9 receptor for CpG ODN C and TLR3 for Poly(I:C).

The lipid-based nanoparticle charge affect the release from GelMA, which has a slightly negative charge (Kim et al., 2022). Lip/Poly(I:C) has the most negative charge and was released faster from the implants than Lip or Lip/CpG ODN C. Lip and Lip/CpG ODN C have a similar surface charge and showed a similar release profile from implants.

4.2. The immune-stimulatory effects of lipid-based nanoparticles

The immunostimulatory assay showed that macrophage secretion of TNF, IL-6, and IL-10 was increased when stimulated with nucleic acids encapsulated in lipid-based nanoparticles compared to their free-form, suggesting delivery using lipid-based nanoparticles was effective. Interestingly, empty lipid-based nanoparticles (Lip) stimulated some cytokine secretion by macrophages. Possible explanations include the activated state of macrophages following a phagocytic stimulus (Fu and Harrison, 2021), the possible immune stimulation by the lipid components (e.g., cationic lipids and ionizable lipid) (Lee et al., 2023), and lastly studies have reported that particle size, charge, or rigidity can affect immune cell behavior (Catenacci et. al., 2024). Future studies could include measurement for a more specific downstream mediator of TLR3 and TLR9, such as interferons (IFN), which can provide a distinction with the immune-stimulatory profile induced by empty lipid-based nanoparticle (Alexopoulou et al., 2001; Krieg, 2002).

CpG ODN C, but not Poly(I:C), showed a positive effect on osteoblast differentiation of hMSCs. hMSCs cultured with conditioned medium from macrophages stimulated with the highest concentration of CpG ODN C (10 μg/ml) and all concentrations of Lip/CpG ODN C (0.1-10 μg/ml) increased in their alkaline phosphatase (ALP) activity by 2.6-fold and 3-fold, respectively. ALP is secreted by pre-osteoblastic cells and, therefore considered as an indicator for early differentiation of MSCs towards the osteoblastic lineage. This aligns with findings from earlier studies showing enhanced osteoblast differentiation of hMSCs when cultured in conditioned medium from peripheral blood mononuclear cells (PBMC) stimulated with CpG ODN C, but not with medium from PBMC alone or stimulated with Poly(I:C) (Khokhani et al., 2022). These findings suggest that CpG ODN C performed better when encapsulated in a lipid-based nanoparticle and that the immune profile generated by TLR9 activation, the receptor for CpG ODN C, has the potential to induce an osteoimmunomodulatory effect, at least *in vitro*.

4.3. Ectopic bone formation in implants

Extra-skeletal (ectopic) bone induction does not occur under normal conditions, and therefore a challenging model for evaluating bone graft substitutes. With no contact with native bone tissue, progenitor cells must be recruited to the implant site and differentiate into osteoblast and osteoclast. In rabbits, bone induction at ectopic locations hardly occurs except if combined with a stimulus such as BMP-2 (Croes et al., 2017). In a pilot study, a marginal dose of BMP-2 on plain BCP led to an average of 5 % bone volume when implanted intramuscularly for 5 weeks (Suppl. Fig. S1). Accordingly, we applied a similar dosage in this study to be able to discriminate the effect of microbial nucleic acids on bone formation in two directions: inhibition or promotion of bone tissue. However, our results indicate no differences in bone volume between the control and experimental groups.

Various studies have reported how inflammation can enhance or inhibit bone formation *in vivo* (Croes et al., 2018, 2019; 2017; Shi et al.,

2018). Despite this, our data showed all groups to perform similarly in terms of ectopic bone formation. One possible explanation is the dose of microbial nucleic acids employed was inadequate to induce a relevant inflammatory response. To mimic the positive observation seen *in vitro*, we administered a comparable working concentration for the intramuscular implant model. However, the literature reports that differences in ligand recognition profiles can occur between species. In a comparative study on the interaction between CpG ODN and TLR9 of different species, it was found that rabbit's TLR9 exhibited a broad ligand-recognition profile—allowing it to bind to numerous variations of CpG ODNs— but its activation is concentration-dependent (Liu et al., 2012). A concentration of at least twice what is required for human TLR9 activation was necessary to achieve comparable levels of activation. Although no comparative study was reported for Poly(I:C) or TLR3 in rabbits, we suggest that differences in the species-related TLR recognition profile might explain our findings.

Additionally, the activity of BMP-2 in this model could have masked the immune-stimulatory effects. Despite applying a marginal dose of BMP-2 and a shorter incubation period than in previous studies (Croes et al., 2018, 2017), we observed the formation of multiple layers of new bone tissue in all implants at week 5. Furthermore, mineralization was evident as early as 3 weeks after implantation, as indicated by fluorochrome deposition (Fig. 4E). We suggest future studies using a similar animal model, to employ a lower BMP-2 dosage.

4.4. Limitations and future perspective

A limitation of this study is the absence of *in vivo* measurements of the local immune response. This requires early sample collection, within the first week, to assess differences in the immune response profile induced by the different groups. Additionally, *ex vivo* methods could be applied to overcome the challenge of translating the optimum working concentrations of PAMPs from an *in vitro* setup to animal studies. Techniques such 'whole blood assay' to asses cytokine production, can provide information on species-dependent TLR activation (Thurm and Halsey, 2005). In addition, multicellular *in vitro* models that take into account the opsonization of antigens by serums' complement proteins into cocultures of MSCs and macrophages (Cecotto et al., 2023) can better demonstrate *in vitro* osteoimmunomodulatory properties.

5. Conclusion

Exploring the use of synthetic PAMPs to activate PRRs presents a fascinating avenue for engineering bone biomaterials with immune-interacting properties. We demonstrated that encapsulating nucleic acid PAMPs in lipid-based nanoparticles improved immune cell activation, indirectly promoting osteoblast differentiation *in vitro*. CpG ODN C encapsulated in lipid-based nanoparticles holds potential as a bioactive agent for osteoimmunomodulation, although further *in vivo* demonstration should corroborate the current *in vitro* findings.

CRediT authorship contribution statement

N.R. Rahmani: Writing – original draft, Visualization, Methodology, Investigation, Formal analysis, Data curation. **F. Jahanmard:** Writing – review & editing, Methodology, Investigation, Formal analysis, Data curation, Conceptualization. **A. Hassani Najafabadi:** Writing – review & editing, Formal analysis. **J. Flapper:** Methodology, Investigation, Formal analysis. **O. Dogan:** Methodology, Investigation, Formal analysis, Data curation. **A. Khodaei:** Investigation, Formal analysis, Data curation. **G. Storm:** Writing – review & editing, Supervision, Conceptualization. **M. Croes:** Writing – review & editing, Supervision, Methodology, Funding acquisition, Conceptualization. **M.C. Kruyt:** Writing – review & editing, Funding acquisition, Formal analysis. **D. Gawlitta:** Writing – review & editing, Formal analysis. **H. Weinans:** Writing – review & editing, Supervision, Funding acquisition, Formal analysis. **E. Mastrobattista:** Writing – review & editing, Supervision, Resources, Funding acquisition, Formal analysis, Conceptualization. **S. Amin Yavari:** Writing – review & editing, Supervision, Resources, Funding acquisition, Formal analysis, Conceptualization.

Declaration of competing interest

The authors declare no competing interests.

Acknowledgement

Schematic illustrations in the article were created with Biorender.com.

Funding sources

The research for this paper was financially supported by the Phospholipid Research Center (PRC) and the EU's H2020 research and innovation program under Marie S. Curie Cofund RESCUE (grant agreement no. 801540).

Supplementary materials

Supplementary material associated with this article can be found, in the online version, at doi:10.1016/j.ejps.2025.107050.

Data availability

Data will be made available on request.

References

Albertsen, C.H., Kulkarni, J.A., Witzigmann, D., Lind, M., Petersson, K., Simonsen, J.B., 2022. The role of lipid components in lipid nanoparticles for vaccines and gene therapy. Adv. Drug Deliv. Rev. 188, 114416. https://doi.org/10.1016/j.addr.2022.114416.

Alexopoulou, L., Holt, A.C., Medzhitov, R., Flavell, R.A., 2001. Recognition of double-stranded RNA and activation of NF-κb by toll-like receptor 3. Nature 413, 732–738. https://doi.org/10.1038/35099560.

Ammi, R., De Waele, J., Willemen, Y., Van Brussel, I., Schrijvers, D.M., Lion, E., Smits, E. L.J., 2015. Poly(I:C) as cancer vaccine adjuvant: knocking on the door of medical breakthroughs. Pharmacol. Ther. 146, 120–131. https://doi.org/10.1016/j.pharmthera.2014.09.010.

Bligh, E.G., Dyer, W.J., 1959. A rapid method of total lipid extraction and purification. Can. J. Biochem. Physiol. 37 (8), 911–917. https://doi.org/10.1139/o59-099.

Bozzuto, G., Molinari, A., 2015. Liposomes as nanomedical devices. Int. J. Nanomed. 10, 975–999. https://doi.org/10.2147/IJN.S68861.

Catenacci, L., Rossi, R., Sechi, F., Buonocore, D., Sorrenti, M., Perteghella, S., Peviani, M., Bonferoni, M.C., 2024. Effect of lipid nanoparticle physico-chemical properties and composition on their interaction with the immune system. Pharmaceutics 16, 1521. https://doi.org/10.3390/pharmaceutics16121521.

Cecotto, L., Stapels, D.A.C., van Kessel, K.P.M., Croes, M., Lourens, Z., Vogely, H.C., van der Wal, B.C.H., van Strijp, J.A.G., Weinans, H., Amin Yavari, S., 2023. Evaluation of silver bio-functionality in a multicellular in vitro model: towards reduced animal usage in implant-associated infection research. Front. Cell Infect. Microbiol. 13.

Chen, Z., Klein, T., Murray, R.Z., Crawford, R., Chang, J., Wu, C., Xiao, Y., 2016. Osteoimmunomodulation for the development of advanced bone biomaterials. Mater. Today 19, 304–321. https://doi.org/10.1016/j.mattod.2015.11.004.

Croes, M., Boot, W., Kruyt, M.C., Weinans, H., Pouran, B., van der Helm, Y.J.M., Gawlitta, D., Vogely, H.C., Alblas, J., Dhert, W.J.A., Öner, F.C., 2017. Inflammation-induced osteogenesis in a rabbit tibia model. Tissue Eng. Part C 23, 673–685. https://doi.org/10.1089/ten.tec.2017.0151.

Croes, M., Kruyt, M.C., Boot, W., Pouran, B., Braham, M.V., Pakpahan, S.A., Weinans, H., Vogely, H.C., Fluit, A.C., Dhert, W.J., Alblas, J., Öner, F.C., 2019. The role of bacterial stimuli in inflammation-driven bone formation. Eur. Cell Mater. 37, 402–419. https://doi.org/10.22203/eCM.v037a24.

Croes, M., Kruyt, M.C., Groen, W.M., Van Dorenmalen, K.M.A., Dhert, W.J.A., Öner, F.C., Alblas, J., 2018. Interleukin 17 enhances bone morphogenetic protein-2-induced ectopic bone formation. Sci. Rep. 8. https://doi.org/10.1038/s41598-018-25564-9.

Croes, M., Oner, F.C., Kruyt, M.C., Blokhuis, T.J., Bastian, O., Dhert, W.J.A., Alblas, J., 2015. Proinflammatory mediators enhance the osteogenesis of Human mesenchymal stem cells after lineage commitment. PLoS ONE 10, e0132781. https://doi.org/10.1371/journal.pone.0132781.

Croes, M., Öner, F.C., van Neerven, D., Sabir, E., Kruyt, M.C., Blokhuis, T.J., Dhert, W.J. A., Alblas, J., 2016. Proinflammatory T cells and IL-17 stimulate osteoblast differentiation. Bone 84, 262–270. https://doi.org/10.1016/j.bone.2016.01.010.

Cypher, T.J., Grossman, J.P., 1996. Biological principles of bone graft healing. J. Foot Ankle Surg. 35, 413–417. https://doi.org/10.1016/S1067-2516(96)80061-5.

De Temmerman, M.-L., Rejman, J., Demeester, J., Irvine, D.J., Gander, B., De Smedt, S. C., 2011. Particulate vaccines: on the quest for optimal delivery and immune response. Drug Discov. Today 16, 569–582. https://doi.org/10.1016/j.drudis.2011.04.006.

Fu, Y.L., Harrison, R.E., 2021. Microbial phagocytic receptors and their potential involvement in cytokine induction in macrophages. Front. Immunol. 12.

Gillman, C.E., Jayasuriya, A.C., 2021. FDA-approved bone grafts and bone graft substitute devices in bone regeneration. Mater. Sci. Eng. C 130, 112466. https://doi.org/10.1016/j.msec.2021.112466.

Guihard, P., Danger, Y., Brounais, B., David, E., Brion, R., Delecrin, J., Richards, C.D., Chevalier, S., Rédini, F., Heymann, D., Gascan, H., Blanchard, F., 2012. Induction of osteogenesis in mesenchymal stem cells by activated monocytes/macrophages depends on oncostatin M signaling. Stem Cells 30, 762–772. https://doi.org/10.1002/stem.1040.

Hafner, A.M., Corthésy, B., Merkle, H.P., 2013. Particulate formulations for the delivery of poly(I:C) as vaccine adjuvant. Adv. Drug Deliv. Rev. 65, 1386–1399. https://doi.org/10.1016/j.addr.2013.05.013.

Hu, M., Li, X., You, Z., Cai, R., Chen, C., 2024. Physiological barriers and strategies of lipid-based nanoparticles for nucleic acid drug delivery. Adv. Mater. 36, 2303266. https://doi.org/10.1002/adma.202303266.

Jahanmard, F., Khodaei, A., Flapper, J., Dogan, O., Roohi, K., Taheri, P., Weinans, H., Storm, G., Croes, M., Mastrobattista, E., Amin Yavari, S., 2023. Osteoimmunomodulatory GelMA/liposome coatings to promote bone regeneration of orthopedic implants. J. Control Release 358, 667–680. https://doi.org/10.1016/j.jconrel.2023.05.022.

Jeffs, L.B., Palmer, L.R., Ambegia, E.G., Giesbrecht, C., Ewanick, S., MacLachlan, I., 2005. A scalable, extrusion-free method for efficient liposomal encapsulation of plasmid DNA. Pharm. Res. 22, 362–372. https://doi.org/10.1007/s11095-004-1873-z.

Kato, H., Takeuchi, O., Sato, S., Yoneyama, M., Yamamoto, M., Matsui, K., Uematsu, S., Jung, A., Kawai, T., Ishii, K.J., Yamaguchi, O., Otsu, K., Tsujimura, T., Koh, C.-S., Reis e Sousa, C., Matsuura, Y., Fujita, T., Akira, S., 2006. Differential roles of MDA5 and RIG-I helicases in the recognition of RNA viruses. Nature 441, 101–105. https://doi.org/10.1038/nature04734.

Kay, R.R., 2021. Macropinocytosis: biology and mechanisms. Cells Dev. 168, 203713. https://doi.org/10.1016/j.cdev.2021.203713.

Khokhani, P., Belluomo, R., Croes, M., Gawlitta, D., Kruyt, M.C., Weinans, H., 2022. An In vitro model to test the influence of immune cell secretome on mesenchymal stromal cell osteogenic differentiation. Tissue Eng. Part C 28, 420–430. https://doi.org/10.1089/ten.tec.2022.0086.

Kim, Y.-H., Dawson, J.I., Oreffo, R.O.C., Tabata, Y., Kumar, D., Aparicio, C., Mutreja, I., 2022. Gelatin methacryloyl hydrogels for musculoskeletal tissue regeneration. Bioengineering 9, 332. https://doi.org/10.3390/bioengineering9070332.

Kitaori, T., Ito, H., Schwarz, E.M., Tsutsumi, R., Yoshitomi, H., Oishi, S., Nakano, M., Fujii, N., Nagasawa, T., Nakamura, T., 2009. Stromal cell–derived factor 1/CXCR4 signaling is critical for the recruitment of mesenchymal stem cells to the fracture site during skeletal repair in a mouse model. Arthrit. Rheumat. 60, 813–823. https://doi.org/10.1002/art.24330.

Krieg, A.M., 2002. CpG motifs in bacterial DNA and their immune effects. Annu. Rev. Immunol. 20, 709–760. https://doi.org/10.1146/annurev.immunol.20.100301.064842.

Lee, Y., Jeong, M., Park, J., Jung, H., Lee, H., 2023. Immunogenicity of lipid nanoparticles and its impact on the efficacy of mRNA vaccines and therapeutics. Exp. Mol. Med. 55, 2085–2096. https://doi.org/10.1038/s12276-023-01086-x.

Lim, J.P., Gleeson, P.A., 2011. Macropinocytosis: an endocytic pathway for internalising large gulps. Immunol. Cell Biol. 89, 836–843. https://doi.org/10.1038/icb.2011.20.

Liu, J., Xu, C., Liu, Y.-L., Matsuo, H., Hsieh, R.P., Lo, J.-F., Tseng, P.-H., Yuan, C.-J., Luo, Y., Xiang, R., Chuang, T.-H., 2012. Activation of rabbit TLR9 by different CpG-ODN optimized for mouse and human TLR9. Comp. Immunol. Microbiol. Infect. Dis. 35, 443–451. https://doi.org/10.1016/j.cimid.2012.03.008.

Medzhitov, R., 2007. Recognition of microorganisms and activation of the immune response. Nature 449, 819–826. https://doi.org/10.1038/nature06246.

Müller, M., Fisch, P., Molnar, M., Eggert, S., Binelli, M., Maniura-Weber, K., Zenobi-Wong, M., 2020. Development and thorough characterization of the processing steps of an ink for 3D printing for bone tissue engineering. Mater. Sci. Eng. C 108, 110510. https://doi.org/10.1016/j.msec.2019.110510.

Ono, T., Okamoto, K., Nakashima, T., Nitta, T., Hori, S., Iwakura, Y., Takayanagi, H., 2016. IL-17-producing γδ T cells enhance bone regeneration. Nat. Commun. 7, 10928. https://doi.org/10.1038/ncomms10928.

Pennings, I., van Dijk, L.A., van Huuksloot, J., Fledderus, J.O., Schepers, K., Braat, A.K., Hsiao, E.C., Barruet, E., Morales, B.M., Verhaar, M.C., Rosenberg, A.J.W.P., Gawlitta, D., 2019. Effect of donor variation on osteogenesis and vasculogenesis in hydrogel cocultures. J. Tissue Eng. Regen. Med. 13, 433–445. https://doi.org/10.1002/term.2807.

Rahmani, N.R., Duits, A., Croes, M., Lock, O., Gawlitta, D., Weinans, H., Kruyt, M.C., 2024. Incorporating microbial stimuli for osteogenesis in a rabbit posterolateral spinal fusion model. Tissue Eng. Part A. https://doi.org/10.1089/ten.TEA.2024.0064.

Rouser, G., Fleischer, S., Yamamoto, A., 1970. Two dimensional thin layer chromatographic separation of polar lipids and determination of phospholipids by phosphorus analysis of spots. Lipids 5, 494–496. https://doi.org/10.1007/BF02531316.

Semple, S.C., Akinc, A., Chen, J., Sandhu, A.P., Mui, B.L., Cho, C.K., Sah, D.W.Y., Stebbing, D., Crosley, E.J., Yaworski, E., Hafez, I.M., Dorkin, J.R., Qin, J., Lam, K., Rajeev, K.G., Wong, K.F., Jeffs, L.B., Nechev, L., Eisenhardt, M.L., Jayaraman, M., Kazem, M., Maier, M.A., Srinivasulu, M., Weinstein, M.J., Chen, Q., Alvarez, R., Barros, S.A., De, S., Klimuk, S.K., Borland, T., Kosovrasti, V., Cantley, W.L., Tam, Y. K., Manoharan, M., Ciufolini, M.A., Tracy, M.A., de Fougerolles, A., MacLachlan, I., Cullis, P.R., Madden, T.D., Hope, M.J., 2010. Rational design of cationic lipids for siRNA delivery. Nat. Biotechnol. 28, 172–176. https://doi.org/10.1038/nbt.1602.

Shi, Y., Wang, L., Niu, Y., Yu, N., Xing, P., Dong, L., Wang, C., 2018. Fungal component coating enhances titanium implant-bone integration. Adv. Funct. Mater. 28, 1804483. https://doi.org/10.1002/adfm.201804483.

Sims, N.A., 2021. Influences of the IL-6 cytokine family on bone structure and function. Cytokine 146, 155655. https://doi.org/10.1016/j.cyto.2021.155655.

Tang, M., Tian, L., Luo, G., Yu, X., 2018. Interferon-gamma-mediated osteoimmunology. Front. Immunol. 9.

Thurm, C.W., Halsey, J.F., 2005. Measurement of cytokine production using whole blood. Curr. Protoc. Immunol. 66. https://doi.org/10.1002/0471142735.im0718bs66, 7.18B.1-7.18B.12.

Van Den Bulcke, A.I., Bogdanov, B., De Rooze, N., Schacht, E.H., Cornelissen, M., Berghmans, H., 2000. Structural and rheological properties of methacrylamide modified gelatin hydrogels. Biomacromolecules 1, 31–38. https://doi.org/10.1021/bm990017d.

Van Dijk, L.A., Barbieri, D., Barrère-de Groot, F., Yuan, H., Oliver, R., Christou, C., Walsh, W.R., de Bruijn, J.D., 2019. Efficacy of a synthetic calcium phosphate with submicron surface topography as autograft extender in lapine posterolateral spinal fusion. J. Biomed. Mater. Res. Part B 107, 2080–2090. https://doi.org/10.1002/jbm.b.34301.

Vermette, P., Griesser, H.J., Kambouris, P., Meagher, L., 2004. Characterization of surface-immobilized layers of intact liposomes. Biomacromolecules 5, 1496–1502. https://doi.org/10.1021/bm049941k.